Optimal manoeuvres with very flexible wings

Salvatore Maraniello*, Robert J. S. Simpson† and Rafael Palacios‡
Imperial College, London, SW7 2AZ, United Kingdom

The single shooting method is used identify optimal manoeuvres in the lateral dynamics of partially-supported wings of very low stiffness. The aim is to identify actuation strategies in the design of aircraft manoeuvres in which large wing deflections can substantially modify the vehicle structural and aerodynamic features. Preliminary studies are presented for a representative high-altitude long-endurance aircraft wing in hinged configuration. Nonlinear effects due to large deflections are captured coupling a geometrically exact beam model with an unsteady vortex lattice method for the aerodynamics. The optimal control problem is solved via a gradient-based algorithm. When lowering the wing stiffness, the nonlinearities connected to the system — such as the fore-shortening effect due to large bending deflections — increase the wing lateral stability but at the same time they also reduce aileron authority. The single-shooting optimisation is shown to capture these features and to provide satisfactory results, not only when refining a predetermined actuation law but also when designing it from zero.

Nomenclature

CRV Cartesian rotation vector
CVP Control vector parametrisation
FoR Frame of reference
GEBM Geometrically-exact beam model
UVLM Unsteady Vortex lattice method

Symbols

β Ailerons deflection
Φ_n n-th basis function of the control parametrisation
σ Wing stiffness parameter
τ_n n-th control point used for the B-splines parametrisation

A Body-attached frame of reference
B Local frame of reference defined along the beam mean axis s
c Column vector for the optimisation problems constrains
G Global frame of reference
I Cost function for the optimisation problems
L Wing half span length
m Order of B-spline basis
N_τ Number of control points for the B-spline parametrisation
N_c Size of the basis used to parametrise the control
R Residual form of the physical system

*Graduate Student, Department of Aeronautics, 363 Roderic Hill Building; salvatore.maraniello10@imperial.ac.uk.
†Graduate Student, Department of Aeronautics, 363 Roderic Hill Building; r.simpson11@imperial.ac.uk. AIAA Student Member.
‡Reader, Department of Aeronautics, 355 Roderic Hill Building; r.palacios@imperial.ac.uk. AIAA Member.

s	Beam mean axis
T	Final time of the dynamic simulations
t	Time
u	Control function
x	Column vector containing the design variables for the optimisation problems
y	Physical system state

I. Introduction

Historically, aeronautical design has been characterised by relatively stiff structures exhibiting relatively small structural deformations. The design of flight control laws for conventional aircraft has been, therefore, usually based on linearised models around a reference flying condition. Typically, the first step of this process consists in linearising the rigid body dynamic equations associated to the vehicle, which allows to express changes of the rigid vehicle attitude in the form of a linear time invariant system. If deformations are small, the gains of such a system can be corrected to account for flexibility effects performing a linear aeroelastic analysis of the reference configuration itself. For years these approaches have been successfully applied to both the control design and stability analysis of conventional aircraft configurations.[1]

As high-efficiency requirements are pushing for lighter and more slender designs, wings of novel aircraft concepts are likely to exhibit large geometrical deformations. The design and manoeuvring of these aircraft presents a number of additional challenges with respect to conventional, stiffer, vehicles.[2] In first instance the higher structural flexibility has the direct effect of lowering the elastic modes natural frequencies, thus strengthening the coupling between flexible and rigid body dynamics. Due to the high flexibility, moreover, large geometrical changes — that significantly impact the wing aerodynamic performance and the overall vehicle stability features — occur not only within different points of the flight envelope but also during a single manoeuvre.

In this context, classical approaches for open-loop control laws design and stability analysis may require adjustments. A typical solution for stability and flutter analysis consists on linearising the aeroelastic system around a fixed trimmed configuration, so as to account for changes in the aeroelastic features of the vehicle if large deflections are present.[3] This process, in particular, needs to be repeated for each point of the flight envelope. In a similar way, and under the same assumption of small displacements with respect to the reference deformed shape, flight control laws can be designed. These approaches are, however, better suitable for those cases in which the desired flight conditions are easily determined, such as when the aim is to design a control to ensure steady flight conditions[4]. In the attempt of seeking for optimal performance, however, a methodology should potentially allow large changes in geometry — and thus in dynamical features — during the manoeuvre itself and, in general, be able to deal with the nonlinear behaviour of a flexible wing as an opportunity for extra performance, rather than a constraint. Previous works aimed to address this point focusing on the development of feedback control laws for trajectory control.[5]

With the aim of maximising the performance of a nonlinear system that can exhibit complex and unintuitive behaviours, the task of designing aircraft manoeuvres via very flexible wings can, instead, be recast as an open-loop optimal control problem where the unknowns are the time histories of the wing aerodynamic control surfaces. In theory, these problems can be solved enforcing an optimality condition on the equations describing the system dynamics (e.g. Pontryagin's principle).[1;6] However, this approach would be too complex — with respect to both the analytical and numerical development — to be applied to the coupled nonlinear flexible-rigid body flight dynamic model of a flexible aircraft. A way around consists, instead, in parametrising the control signal and solving the problem numerically via nonlinear programming techniques for optimisation (direct methods). Single and multiple shooting methods, in particular, are directly linked to single and multidisciplinary optimisation (MDO): once a parametrisation is chosen, in fact, the coefficients of the parametrisation are directly handled by the optimisation algorithm.[7] An appealing feature of this approach is that it can be extended to a combined optimisation problems with relatively little effort: once the actuation is parametrised, in fact, there is no formal difference, at the optimiser level, between the open-loop optimal control solution and the optimisation with respect to any other aircraft design parameter.[6;8]

In this work, an optimisation framework has been built around the aeroelastic simulation environment SHARPy (simulation of high aspect ratio planes in Python).[9–11] The nonlinear aeroelastic solution is obtained by loosely coupling a geometrically exact beam model (GEBM) with an unsteady vortex lattice method (UVLM) for the rigid and flexible vehicle aerodynamics. Both the GEBM and the UVLM have been designed to capture large deflections and, importantly, the fore-shortening effect due to large bending displacements.[12] The coupling between rigid-body and flexible modes dynamics is also accounted for. The aeroelastic model is initially used to assess key manoeuvrability features of flexible wing. To this aim, a model of a high-altitude long-endurance (HALE) representative wing[9;13] in hinged configuration has been built. This set of constraints, in particular, allows to isolate the dynamics associated to the wing flexibility from that of the rest of the aircraft. Finally, using the single shooting (or control vector parametrisation, CVP) technique, the time histories of the wing control surface deflections have been optimised via a gradient based method.

II. Methodology

This section introduces the modelling approach for nonlinear aeroelastic analysis built in SHARPy (Sec. II.A). The main features of the model are the coupling between rigid and flexible body dynamics and the ability to capture the impact on the aerodynamic loads of large deformations during a prescribed manoeuvre. The control surface actuation is approximated by the deflection of the wing panels. Sec. II.B introduces instead the single shooting method as a solution to optimal control problems and describes the set-up chosen for the optimisation.

II.A. Aeroelastic Model

The nonlinear time dependent aeroelastic analysis required to simulate the wing behaviour when, possibly, large geometrical changes occur will be performed within the SHARPy environment.[9–11] The solver, which has been extensively verified in previous studies,[11;14;15] loosely couples a GEBM[16;17] with a free-wake UVLM solver.

The coupled flexible-rigid body dynamic structural model is described using the notation introduced by Hesse et al,[11] with frames of reference (FoRs) and relevant vectors being shown in Fig. 1. The rigid body

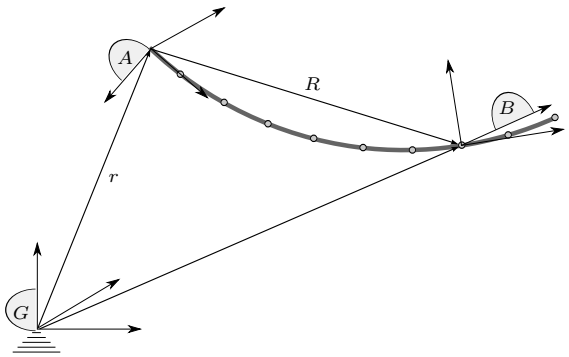

Figure 1: Definition of frames of reference

dynamics is expressed in terms of translational (v_A) and rotational (ω_A) velocity vectors of a FoR attached to the body, A, with respect to the ground FoR G — note that the subscript stands for the FoR in which quantities are projected. In the GEBM local deformations are assumed to be small, thus allowing to use a linear material model. At each section of the beam, force and moment strains are expressed into a local FoR B, defined along the beam mean axis s.[16] As this latter can move and rotate with respect to the body FoR A, large displacements and rotations can be captured accurately. In particular, the local orientation

with respect to the body-fixed axes A is expressed using the Cartesian rotation vector, $\Psi(s)$. The coupled nonlinear rigid body dynamics is finally expressed as:

$$M(\eta)\begin{Bmatrix} \ddot{\eta} \\ \dot{\chi} \end{Bmatrix} + \begin{Bmatrix} Q^s_{gyr}(\eta,\dot{\eta},\chi) \\ Q^r_{gyr}(\eta,\dot{\eta},\chi) \end{Bmatrix} + \begin{Bmatrix} Q^s_{stif}(\eta) \\ 0 \end{Bmatrix} = \begin{Bmatrix} Q^s_{ext}(\eta,\dot{\eta},\zeta,t) \\ Q^r_{ext}(\eta,\dot{\eta},\zeta,t) \end{Bmatrix}, \tag{1}$$

where $\chi^T = \{v_A^T, \omega_A^T\}$, η is a vector containing nodal rotation and displacements, and Q_{gyr}, Q_{stiff}, Q_{ext} are, respectively, gyroscopic, stiffness and external forcing terms.[11] The external force Q_{ext} includes both gravitational and aerodynamic contributions. This is expressed in terms of quaternions such that $\zeta^T = \{\zeta_0, \zeta_v^T\}$. The scalar ($\zeta_0$) and vector ($\zeta_v$) parts of ζ are obtained via integration of FoR A angular velocity ω_A according to:[18]

$$\dot{\zeta_0} = -\frac{1}{2}\omega_A^T\zeta_v \quad , \quad \dot{\zeta_v} = -\frac{1}{2}\left(\zeta_0\omega_A - \tilde{\omega}_A\zeta_v\right) \tag{2}$$

where $(\tilde{\ })$ is the skew symmetric matrix operator. Spherical joint boundary conditions (BCs) have been implemented by setting the velocity of the body FoR v_A to be zero. Hinge BCs can be derived similarly, allowing rotations only along one axis.

The aerodynamic component of the external forcing term Q_{ext} is computed via the UVLM, for which a detailed description is provided by Murua et al.[9] The flow is assumed to be incompressible, inviscid and irrotational, thus allowing to express the velocity field in term of a potential function. These hypothesis are a realistic assumption when dealing with low Mach numbers and fully attached flows. The no separation hypothesis implies that changes in wing geometry occur slowly in respect to the flow characteristic time scales. Under these conditions, the notion of vortex ring can be introduced and used to discretise the aerodynamic surfaces and the wake. Being Γ the circulation strength associate to each of them, the velocity induced by a single vortex can be computed using the Biot-Savart law and the global velocity field can be derived using the superposition principle. At each time step, vorticity is shed at the trailing edge, thus building up the wake. To fully capture the effect of large deformations, in particular, the wake geometry is not prescribed but is computed as part of the solution on the basis of convecting the vortex rings in the wake with the local flow velocity. The vorticity field at the time-step n is solved by enforcing the non-penetration condition at a number of collocation points distributed over the wing, thus leading to:

$$A_b\Gamma_b^n + A_w\Gamma_w^n + w^n = 0 \tag{3}$$

In eq. (3) Γ_b and Γ_w are the surface (bound) and wave strength circulation vectors, while A_b and A_w are the wing-wing and wing-wake aerodynamics influence coefficients matrices. The first two terms in eq. (3) return the velocity induced by the vortex rings system on the collocation points, while the vector w contains the normal velocity of the collocation points due to the wing deformations and rigid body motion, as well as the movement of aerodynamic control surfaces and gust induced velocity. The third term determines the coupling with the structural and control disciplines. Once the vorticity is solved for, the global velocity field can be computed and used to derive the forces on the vortex rings — and thus the aerodynamic loads — by means of Joukowski's theorem.[10] These lead to an expression for the aerodynamic component of the external forcing term Q_{ext} appearing in eq. (1), thus closing the coupling between structural and aerodynamic solvers.

II.B. Optimal Control via Single Shooting

The optimal control of a flexible aircraft can be seen as an optimisation problem in which the design variable is a time-dependent function, the control input $u(t)$. This can be written in standard form as:

$$\begin{aligned} \text{minimise} \quad & I = I(u, y, \dot{y}) \\ \text{with respect to} \quad & u(t), y(t) \\ \text{subject to} \quad & c(u, y) \geq 0 \\ & R(t, u, y, \dot{y}) = 0 \end{aligned} \tag{4}$$

In problem (4) $y = \{\eta, \chi, \zeta, \Gamma_b, \Gamma_w\}^T$ is the state of the aeroelastic system, I is the cost functional to minimise while c and R define design and discipline constraints. The set of equations R is linked instead to the solution of the aeroelastic system defined by eq. (1), (2) and (3) over the time horizon $[0, T]$. The design constraints $c = \{c_o, c_c\}$, can be used to meet control specific (c_c) and general (c_o) design requirement. In this work the control input at time t is provided by the ailerons deflection $\beta(t)$ and bound constraints are enforced to limit both their amplitude and rate of change:

$$\begin{matrix} |\beta(t)| \leq \beta_{max}(t) \\ |\dot{\beta}(t)| \leq \dot{\beta}_{max}(t) \end{matrix} \quad , \quad t \, \epsilon \, [0, T] \tag{5}$$

In direct transcription (DT) deriving methods, both state and control are discretised in time and treated as design variables. From a MDO point of view, the method is equivalent to an all-at-once (AAO) or simultaneous analysis and optimisation (SAND) architecture, with the optimiser solving for the physics and optimal control simultaneously. While DT deriving methods are capable to explore infeasible and unstable states, thus possibly leading to a faster convergence of the optimisation, the number of design variables is drastically increased and convergence issues are also likely to arise when integrating the approach in a multidisciplinary analysis context.

Here the aeroelastic analysis is solved at each iteration for the state, y, and problem (4) can be recast in the form of a multidisciplinary feasible architecture (MDF),[19]

$$\begin{aligned} \text{min.} \quad & I = I\left(u, y(u), \dot{y}(y, u)\right) \\ \text{w.r.t.} \quad & u \\ \text{s.t.} \quad & c_o(u, y(u)) \geq 0 \\ & c_c(u, y(u)) \geq 0 \end{aligned} \tag{6}$$

where the dependency of the state on the control, $y = y(u)$, has been explicitly stated. In the single shooting approach, the control signal is expressed as a linear combination of N_c basis functions, $\phi_n(t)$, defined over the time horizon $[0, T]$:

$$u = \sum_{n=1}^{N_c} u_n \; \phi_n(t) \tag{7}$$

and the optimisation problem (6) is solved with respect to the coefficients of the parametrisation, u_n. In most control problems, a piecewise constant parametrisation is used: in addition to being easy to implement, this scheme offers good convergence properties.[7] However, to describe the movement of typical control actuators on a relatively large time domain, piecewise constant or linear parametrisations would lead to set of basis functions of substantial size. While from a computational point of view adjoint methods can deal effectively with an increased numbers of design variables, these present the additional development cost of building the adjoint model itself.

With the purpose of modelling smooth actuation signals while limiting the number of coefficients used to parametrise the control, N_c, only $\mathcal{C}^1$ continuous or higher parametrisations were considered for this work. In particular, B-splines have been chosen for their smoothness properties.[8] A set of B-splines basis functions of order p can be built recursively over a set of N_τ control points τ_n as:[20]

$$\phi_n^{(0)}(t) = \begin{cases} 1 & \text{if } \tau_n < t < \tau_{n+1} \\ 0 & \text{else} \end{cases} \tag{8}$$

and

$$\phi_n^{(p)}(t) = \frac{t - \tau_n}{\tau_{n+p} - \tau_n} \phi_n^{(p-1)}(t) + \frac{\tau_{n+p+1} - t}{\tau_{n+p+1} - \tau_{n+1}} \phi_{n+1}^{(p-1)}(t) \quad p > 0 \tag{9}$$

Note that, if N_τ control points are used, the number of spline basis required is $N_c = N_\tau + p - 1$. Convergence studies have showed that third order B-splines provide good and smooth reconstructions for the applications in this work. The frequency range of actuation can be regulated by noticing that, in order to capture a maximum frequency f_{max}, a spacing between control points $\Delta\tau = 1/2f_{max}$ is necessary (Nyquist criterion).

In line with previous works in optimal control of dynamical systems[20;21] a standard quasi-Newton method, the SLSQP optimisation algorithm,[22] has been used to solve the final optimal control problem. The implementation is monolithic and uses finite differences for the gradient evaluation. In all the problems considered, cost and constraint functions, as well as design parameters, are scaled to achieve comparable orders of magnitude. If all the constraints are verified, the optimisation process is stopped whenever the relative change in cost and constrains is below a tolerance value of 0.1%.

III. Numerical Studies

In the first part of this section, key aspects of rolling manoeuvrability using flexible wings are investigated. To isolate the dynamics associated to the wing flexibility, a model of a hinged HALE wing has been created (Sec. II.A). The rolling performance for a prescribed aileron deflection are then analysed in Sec. III.B when lowering the stiffness of the wing itself. This section, in particular, outlines how large bending deflection and asymmetric deformations affect the rolling performance. Finally, it is shown in Sec. III.C how the single shooting can be used to define aileron deflection time histories for manoeuvring the wing.

III.A. Wing Model Description

With the aim of isolating the impact of wing flexibility on the aircraft rolling performance, a model of a wing hinged at its mid-span has been created. This setting allows to block pitch and yaw attitudes, thus stabilising the wing without horizontal and vertical tail planes. Two different set-up are presented. In a first case the wing is simply hinged and invested by the airflow. In the second set-up, the hinged wing is also allowed to move sideways, so as to emulate the impact of side-slip in the manoeuvre. The hinged-wing model is built based on a HALE representative configuration first introduced by Patil et al.[13] As proposed by Murua et al[9] and with the aim of investigating the impact of the wing flexibility on its manoeuvring performance, the stiffness of the original model is parameterised by mean of a stiffness factor, σ. The properties of the resulting model are summarised in Tab. 1. In the studies presented in this work, the stiffness parameter σ is varied in the range $1 \div 10$, where $\sigma = 1$ corresponds to the original configuration proposed by Patil et al.[13] The wing is always assumed to fly at an altitude of 20 km and, unless otherwise specified, at a speed of $25\,\mathrm{m\,s^{-1}}$.

Property	Value	
Chord	1	m
Wing span	32	m
Elastic axis	0.5	m
Inertial axis	0.5	m
Mass per unit length	0.75	$\mathrm{kg\,m^{-1}}$
Moment of inertia	10^{-1}	$\mathrm{kg\,m}$
Extensional stiffness	10^{10}	$\mathrm{N\,m^2}$
Torsional stiffness	$\sigma \cdot 10^4$	$\mathrm{N\,m^2}$
Spanwise bending stiffness	$2\sigma \cdot 10^4$	$\mathrm{N\,m^2}$
Chordwise bending stiffness	$5 \cdot 10^6$	$\mathrm{N\,m^2}$

Table 1: Hinged wing properties.

Large bending deflections, comparable to the wing span, can be observed as the wing flexibility is in-

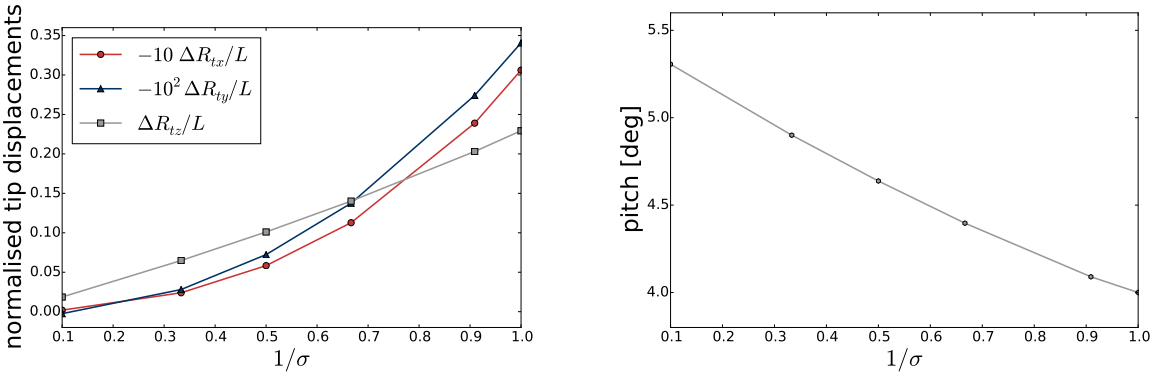

(a) Tip deflection

(b) Angle of attach

Figure 2: Pitch attitude required by wings of different stiffness, flying at a speed of $25\,\mathrm{m\,s^{-1}}$ and an altitude of 20 km, to provide a lift of 488 N and related tip displacements.

creased. This is shown in Fig. 2a, where the wing tip displacements, ΔR_t, for different values of σ are reported. The wings pitch attitude was adjusted so as to produce a lift of 488 N (Fig. 2b). When the wing stiffness is reduced, in fact, larger torsional deformations increase the wing cross-sections local angle of attack, allowing the wing to achieve a considerably higher lifting force. In Fig. 2a all displacements have been normalised with respect to the wing half span length, $L = 16$ m, but the component of displacements in the x (span-wise) and y (chord-wise) directions have been magnified by a factor of 10 and 10^2 respectively. For the $\sigma = 1$ wing the vertical tip deflection reach a maximum value of 0.22 L, which was found to be in good agreement with previous CFD based studies.[23] Compatibly to the stiffness properties defined in Tab. 1, span-wise and chord-wise deflections (ΔR_{tx} and ΔR_{ty}) are, respectively, one and two orders of magnitude smaller then vertical deflections. Nonetheless, it will be shown that these can still contribute to change the handling performance of the wing. In particular, the fore-shortening effect caused by the large bending deformations (up to 3 % of the half wing span for the $\sigma = 1$ wing) reduces the moment arm of the aerodynamic control surfaces, diminishing their control authority. Also the chord-wise displacements can generate a small swept angle (0.20 deg for $\sigma = 1$) that contributes to the lateral stability of the wing.

The onset of flutter was investigated for the $\sigma = 1$ configuration at a pitch attitude of 4 deg and was found to occur over a velocity of $21.4\,\mathrm{m\,s^{-1}}$ with a frequency of 3.27 Hz. These values were found to be in good agreement with those reported by Patil et al[13] — who used a finite-state air-loads model.[24] A cantilever model of the HALE semi-wing, discretised by mean of 16 quadratic beam elements, is used in this study. It is worth mentioning, however, that applying a hinge to the wing does not affect the flutter speed so predicted. This was verified by a time-domain analysis and applying an anti-symmetric aileron deflection so as to excite its anti-symmetric modes. For this study, the wake length was fixed to be 30 times the chords and the airflow speed was increased with steps of $0.1\,\mathrm{m\,s^{-1}}$. The wing panelling and the simulation time-step were chosen so as to ensure an accurate resolution of the range of reduced frequencies for which flutter was expected. No variation in flutter speed was observed for small amplitude ailerons input. When these become large enough to induce relevant changes on the deformed wing shape, however, flutter could be seen to initiate at a lower speed on the semi-wing where tip deflections would be higher. The link between tip deflections and flutter speed has been already reported in literature[13;25] and is not discussed further in this work.

III.B. Impact of Wing Flexibility on Rolling Performance

The rolling performance of hinged flexible wings can now be investigated. All wings are assumed to fly at a speed of $25\,\mathrm{m\,s^{-1}}$ and the pitch attitude has been chosen as per Fig. 2b, so as to ensure that they all produce the same total lift. It is worth noticing that for the most flexible wings ($\sigma < 1.5$) the free stream velocity

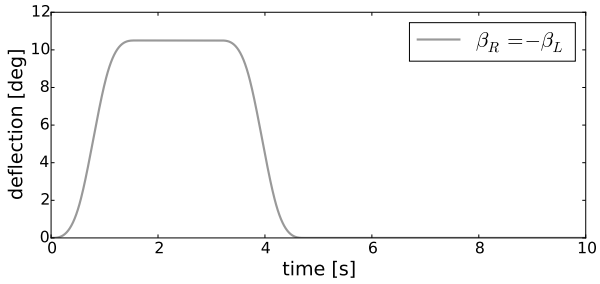

Figure 3: Ailerons deflection used for the study of the rolling manoeuvre performance of flexible wings.

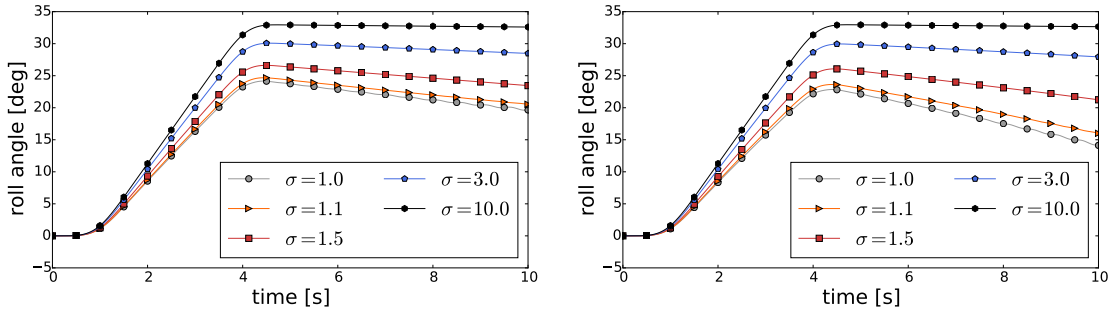

(a) No side-slip

(b) Side-slip

Figure 4: Roll attitude time history for an ailerons antisymmetric deflection with different values of the stiffness parameter σ.

is beyond the flutter boundary. This is high-frequency with respect to the characteristic frequencies of the manoeuvres considered (see Sec. III.A) and could be easily stabilised using a feedback control. However, this was not necessary as the raise time of the instability was always found to be large as compared to the total time of the manoeuvre. These cases were, therefore, included in the study to assess the impact of very large deformations (above 25 % of the semi-wing span) on the wing manoeuvrability. For the numerical analysis, the wing structure has been discretised using 32 quadratic beam elements. The UVLM wake length was fixed to be 25 chords and 4 chord-wise panels were used to discretise the wing surface. Rolling is induced applying an anti-symmetric aileron deflection (Fig. 3) so as to move the right (starboard) wing upwards; the deflections of the left and right control surfaces, β_L and β_R, are assumed to be positive when increasing the local lift.

Fig. 4 shows the roll attitude, measured at the hinge point, of wings of stiffness parameters ranging between $\sigma = 1$ and $\sigma = 10$ with (Fig. 4b) and without (Fig. 4a) side slip effects being accounted for. The maximum side force achieved during the manoeuvre (normalised with respect to the initial lift of 488 N) and the decay rate observed as the wing rolls back to its original attitude are summarised in Tab. 2. In first place, the lateral stability of a rigid ($\sigma = 10$) hinged wing with no dihedral and sweep is briefly discussed. Such a wing is in a neutral equilibrium position with respect to rolling. This is observed in Fig. 4: whether or not side-slip is accounted for, soon after the ailerons are retreated the wing finds a new equilibrium position around a roll angle of 33 deg. In absence of dihedral and sweep angles the side-slip velocity only impacts the lateral force achieved during the manoeuvre: this drops of 6.4 % when the wing is allowed to move side way, due to the reduction in effective angle of attach produced by the relative motion with respect to the air flow (Tab. 2).

With the increase of wing flexibility, two main effects can be observed. In first place, the authority of

σ	Without side slip		With side slip	
	$\max\{F_X/F_Z\}$ [%]	decay rate [$\mathrm{N\,s^{-1}}$]	$\max\{F_X/F_Z\}$ [%]	decay rate [$\mathrm{N\,s^{-1}}$]
1.0	37.7	-5.86	35.3	-10.93
1.1	37.9	-5.37	36.3	-9.27
1.5	39.6	-3.27	38.8	-5.51
2.0	40.7	-1.76	40.2	-4.93
3.0	42.8	-1.07	41.8	-2.73
10.0	45.7	-0.05	44.9	-1.27

Table 2: Maximum side force and decay rate during rolling manoeuvre. The side force is express in percentages of the total lift at the beginning of the manoeuvre (488 N).

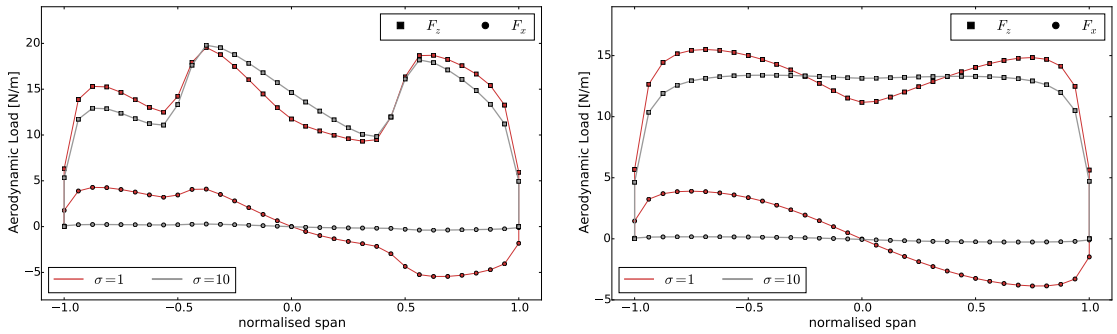

(a) $t = 2$ s (b) $t = 6$ s

Figure 5: Comparison of loads distribution at different times of the rolling manoeuvre for wings having a stiffness of $\sigma = 1$ and $\sigma = 10$.

the control surfaces is reduced: as it can be seen in Fig. 4, the more flexible the wing, the smaller is the roll angle achieved during the manoeuvre. As a result, the side force generated during the manoeuvre drops 17.6 % and 21.3 % (depending on whether side-slip is allowed or not) when going from a very stiff ($\sigma = 10$) to a very flexible ($\sigma = 1$) structural design (Tab. 2). In a second phase, a stabilising moment, which tends to restore the original roll attitude, arises once the ailerons are retreated. Again, this effect intensifies with the increase of geometrical changes and when side-slip motion is allowed. While the stiffer wing ($\sigma = 10$) maintains a constant side force at the end of the manoeuvre, this decays at a rate as high as $10.9\,\mathrm{N\,s^{-1}}$ when the wing becomes very flexible ($\sigma = 1$) and side slip is allowed.

The reduction in control authority can be mainly attributed to the large bending and torsional deformations. Bending deflections are connected to the fore-shortening effect: as these increase, the wing tips get closer to the axis of rotation (see, for instance, the span-wise tip displacements in Fig. 2a) and, consequently, the moment arm available is reduced. The negative impact of large torsional deformations is, instead, more clearly understood by looking at wing loads during the manoeuvre. Fig. 5a compares the aerodynamic loads 2 s into the rolling manoeuvre — when the ailerons are fully deployed and the rolling rate is steady — along the span of a stiff ($\sigma = 10$) and flexible ($\sigma = 1$) wing. To allow a fair comparison, the force components are projected in the body attached FoR A. Larger torsional deformations increase the local angle of attach of the flexible wing cross-section: consequently, while a higher lifting force is obtained on the right, moving upwards, wing, the lift reduction of the left wing is for the same reason limited. This effect results into a loss of rolling moment with respect to the rigid wing. Also the center wing load distribution can be observed to negatively counteract the rolling moment due to the ailerons deflections.

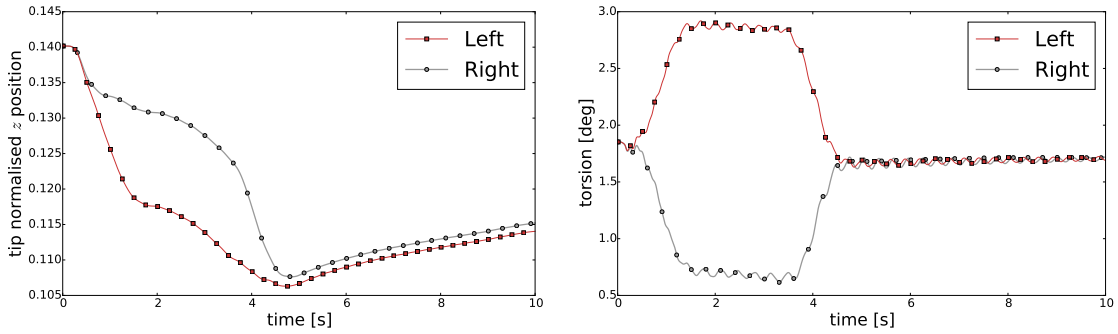

(a) Tip vertical position

(b) Tip torsion

Figure 6: Tip bending deflection (normalised against the semi-wing span) and torsion during a rolling manoeuvre for a wing of stiffness $\sigma = 1.5$.

The mutual interaction between torsional deformations and fore-shortening can, furthermore, amplify the unfavourable influence on the handling of flexible wings. As the wing rolls, in fact, the left wing stretches up as the total aerodynamic load decreases. On the other hand, the starboard wing (which also experiences a small reduction in loads due to the reduction in effective angle of attack associated to the rigid-body rotation and the upward velocity) maintains larger bending deformation and, therefore, a stronger fore-shortening effect. The resulting asymmetry is shown in more detail in Fig. 6a for a wing with stiffness parameter $\sigma = 1.5$: as the wing rolls steadily the difference in tip deflection is at its peak.

The stabilising rolling moment observed once the aileron deflection is returned to zero is also connected to the bending deformations of the wing, which give the wing a dihedral angle. As the axis of rotation is not aligned with the air stream, in fact, the cross sections of the port wing, moving downwards, will tend to have a higher angle of attack than those of the right side of the wing. This can be observed in Fig. 5, where the span-wise aerodynamic load distribution at time $t = 6$ s (i.e. when the ailerons are not loger deflected) is shown for a very flexible ($\sigma = 1$) and an almost rigid wing ($\sigma = 10$). While the stiffer wing shows, as expected, a symmetric loads distribution, the flexible one is characterised by a higher lift on the left wing. It is worth underlining that this effect would also be observed on a rigid wing with dihedral angle, despite the presence of side-slip velocity. However, it would disappear if the wing was rotating about an axis parallel to the free air stream velocity as, in this case, no change in local angle of attack would be connected to bending.

As shown for the reduction in control authority, the asymmetry in the wing deformation contributes to increase the magnitude of the stabilising moment. As seen in Fig. 6a for a $\sigma = 1.5$ wing, as this rolls back to its initial equilibrium position ($t > 4$ s), the port wing remains more stretched. This, together with the effect of the rigid body rotations, guarantees a higher angle of attack then on the right wing. Torsional deformations, on the other hand, do not to contribute significantly to increase the differences between the two sides of the wing. Fig. 6b shows the x component of the CRV at the tips of the $\sigma = 1.1$ wing, which can be used to quantify the torsion at the tip cross-sections. Once the ailerons are returned to a zero angle of attack, no major difference is observed between left and right wing tips. Also gravity does not play a major rule here: for this manoeuvre, in fact, the same stabilising effect is observed without gravity.

All the effects discussed are observed whether side-slip is accounted for or not. When side-slip is allowed, however, the dihedral effect amplifies the restoring moment, causing the decay rate of the total side force to almost double (Tab. 2). The overall restoring moment can become particularly intense as the wing bending deformations become larger. This is shown comparing the response of a $\sigma = 1.1$ and a $\sigma = 10$ wing flying at $30\,\mathrm{m\,s^{-1}}$ to the aileron input in Fig. 3: in this configuration the $\sigma = 1.1$ has tip vertical deflections up to the 30 % of the half winf span L. Note that, in order to stabilise these wings to flutter, their torsional stiffness was increased by a factor of 3. As it can be observed in both Fig. 7 and Fig. 8 where, respectively, the roll attitude and the snapshots of the manoeuvre are shown, the $\sigma = 1.1$ wing eventually returns to its

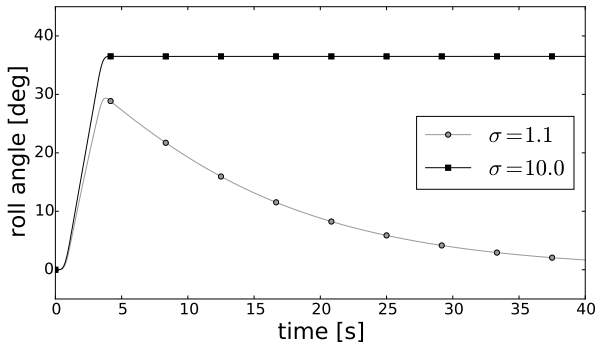

Figure 7: Roll attitude of a rigid ($\sigma = 10$) and a flexible ($\sigma = 1.1$) wing flying at a speed of $30\,\mathrm{m\,s^{-1}}$ in response to the aileron input shown in Fig. 3 and when accounting for side-slip.

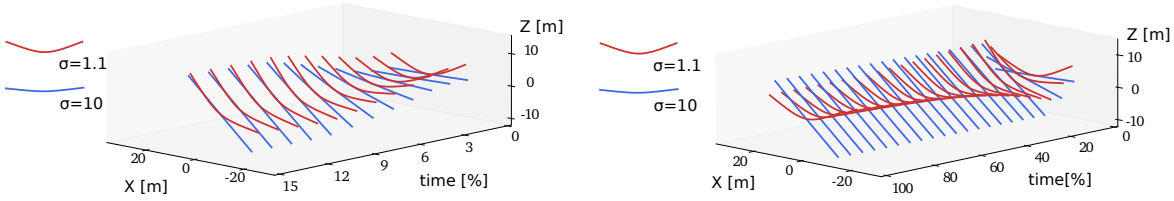

(a) $t\ \epsilon\ [0, 6]$ s

(b) $t\ \epsilon\ [0, 40]$ s

Figure 8: Snapshots of the short and long term response of two wings of stiffness $\sigma = 1.1$ and $\sigma = 10$ to the aileron input shown in Fig. 3 at $30\,\mathrm{m\,s^{-1}}$. Note that the sideways movement of the wing during the manoeuvre is not shown.

original equilibrium position. The snapshots in Fig. 8 help to gather an idea of how strong the dihedral effect can be when large geometrical deformations occur. When the highest roll attitude is reached ($t \approx 6$ s) the right side (moving upwards) of the $\sigma = 1.1$ wing has a very large angle with respect to the horizontal plane — in Fig. 8a its elastic axis can be seen to almost overlap with that of the $\sigma = 10$ wing — and experiences, therefore, a lift reduction due to side slip. The left wing, on the other hand, remains almost parallel to the horizontal plane and is almost unaffected by the lateral velocity generated during the manoeuvre. This unbalance in lift distribution is the additional contribution that intensifies the restoring moment acting on the very flexible wings.

III.C. Optimal Control of Flexible Wings

Results in Sec. III.B have shown that the flight dynamics of flexible wings is substantially more complex compared to that of rigid wings. The larger deflections, in fact, affect the wing manoeuvrability features and make the scheduling of actuation deflection nearly impossible. In this section, the use of the single shooting method is proposed to overcome this extra degree of complexity and design their manoeuvres laws.

To this aim, the time history of the control surfaces deflections has been parametrised via a set of B-splines, as shown in eq. (7), (8) and (9). The optimal manoeuvre can then be obtained as solution to the optimal control problem (6). For this study, the control laws are designed so as to obtain a target lateral force F_r — equal to the 41 % of the initial lift — within a time $t = T_v$ and then to maintain it constant for

a time period T_s. The cost function I has been, therefore, defined as the average relative error

$$I = \frac{1}{T_s} \int_{T_v}^{T_v+T_s} \left| \frac{F_X(t)}{F_r} - 1 \right| dt \quad , \tag{10}$$

where F_X is the lateral aerodynamic force in the global FoR G. The total time for the manoeuvre is $T = T_v + T_s = 7$ s. Bound constraints as per eq. (5) have been used to enforce realistic control surfaces travel limits and a maximum rate of deflection. The limit values were chosen to be $\beta_{max} = 10.5\,\mathrm{deg}$ and $\dot{\beta}_{max} = 15\,\mathrm{deg\,s^{-1}}$. While the aileron deflections at time $t = 0$ s are zero, at time $t = T$ the amplitude required to counteract the stabilising rolling moment is found as a solution of the optimisation problem. The number of basis functions used to represent the actuation signal has a strong impact on the highest frequency that the control can capture.[8] As the focus is on low-frequency dynamics, and in order not to excite the modes of the structure in this exploratory study, the aileron input was parametrised using $N_\tau = 14$ control points (resulting in $N_c = 16$ splines), so as to achieve a maximum nominal excitation frequency of 1 Hz. To investigate the impact of the wing flexibility on the optimal actuation, the rolling manoeuvre is designed for wings of different stiffness parameters. In all cases, they are assumed to be flying at a speed of $25\,\mathrm{m\,s^{-1}}$ and, as per Sec. III.B, the pitch attitude is adjusted to ensure all the wings produce the same lift (Fig. 2b). The ailerons deflection is constrained to be antisymmetric ($\beta_R = -\beta_L$) and the time allowed to reach the target later force, T_v, was chosen to be equal to 75 % and 50 % of the total time of the analysis, so as to test the method for a less and more aggressive control, respectively. Unless otherwise stated, at the beginning of the optimisation the initial aileron deflections time histories are constant and equal to zero.

When a less aggressive control is required, the optimiser manages to achieve a good level of performance for all the cases considered. This is observed in Fig. 10a, where the side force obtained during the manoeuvre is shown for $\sigma = 1.1$ and $\sigma = 3$. The optimal actuations associated to these cases are shown in Fig. 11a: as expected, the loss in authority of the control surfaces on the most flexible wing is compensated by larger levels of actuation. As a result, the side force trends are seen to converge (Fig. 10a) and in both cases the final cost is below 1 %. Nonetheless, a delay in meeting the target side force is observed. In this respect, a comparison with the results obtained with a more aggressive control ($T_v = 50\%\ T$) show that, using larger amplitude ailerons deflections (Fig. 12b), the raise time of the side force can be increases further with both $\sigma = 1.1$ and $\sigma = 3$ (Fig. 10b). The delay observed using the $T_v = 75\%$ control, therefore, is connected to the optimisation process itself and not to the dynamics of the wings.

When the wing flexibility is increased, more aggressive actuations also cause larger amplitude oscillations around the final reference side force F_r (Fig. 10b). These are more clearly visible in the ailerons time histories shown in Fig. 12b and are connected not only to the faster dynamics but also to the fact that a terminal condition on the final state was not specified in the optimal control problem definition. The final cost achieved in these cases ranges between 3 % and 1 %, with the highest values being associated to the most flexible wing designs. In all cases, the roll attitude follows the same trend as the side force (Fig. 11). The impact of a larger flexibility is, however, reflected in the lower roll angle required with $\sigma = 1.1$ to achieve the target side force. As observed in Fig. 5a, in fact, the large bending deflections induce a non negligible lateral component of the aerodynamic force and this effect can be exploited during the manoeuvre.

To further investigate the performance of the method, the impact of the initial guess used is the optimisation is studied. To this aim, the control laws for the $T_v = 50\%\ T$ case are recomputed starting from the actuation time history shown in Fig. 13a (continuous curve). In this problem, the gradient-based optimiser is expected to minimise the cost function I locally. For all the wings considered, the actuation signal is successfully refined (Fig. 13), and the final cost is reduced from 6.1 % to 2.5 % for the $\sigma = 1.1$ case and from 6.9 % to 1.3 % for the $\sigma = 3$ case. These values compare well with those obtained using a zero initial guess, showing that for the manoeuvres considered the design space is smooth enough to allow the use of a gradient-based method to design the actuations laws. A delay in reaching the target side force is still observed. For the most flexible wing ($\sigma = 1.1$) this shows that the wing dynamics is not fast enough — the deflection amplitude and raising time are as large as they can be when $t < T_v$. For the stiffer wing ($\sigma = 3$), on the other hand, the actuation amplitude is not bounded to the maximum constraint, and why the optimiser does not increase it further is still under investigation.

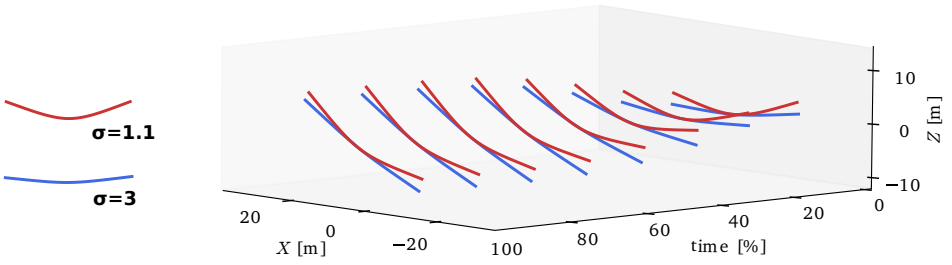

Figure 9: Elastic axis deformations of two wings of different stiffness during the optimal manoeuvre defined using the cost function in eq. (10) and setting $T_v = 50\%\ T$.

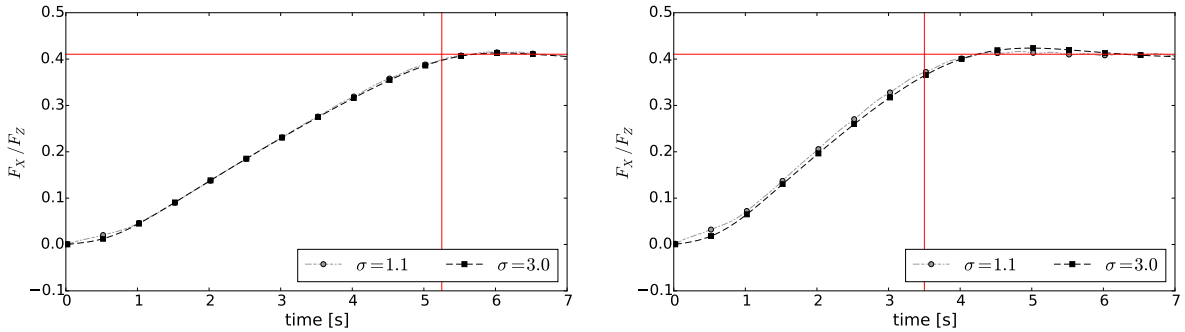

(a) $T_v = 75\%\ T$ (b) $T_v = 50\%\ T$

Figure 10: Aerodynamic side force in response to the optimal anti-symmetric actuation, $\beta_L = -\beta_R$, obtained starting from a zero initial guess and using wings of different stiffness. The plots also show the target lateral force required and the time of average T_v.

Finally, the method is tested to define the control laws for a more complex manoeuvre, aiming, initially, to roll the wing so as to maximise the lateral force F_X in the time interval $[0, T_v]$ and, in a second phase, to restore the wing original attitude. The cost function for the problem has been formulated as follows:

$$I = \int_0^{T_v} F_X dt - \kappa \int_{T_v}^{T_v+T_s} |F_X(t)|\, dt \quad , \tag{11}$$

where $\kappa = 10$ is a scaling parameter and the characteristic times T_v and T_s were chosen to be $T_v = 10$ s and $T_s = 5$ s. For this case, the flying speed was set to $30\,\mathrm{m\,s^{-1}}$ and a wing of stiffness parameter $\sigma = 1.1$ was used (as done in Sec. III.B, its torsional stiffness was increased by a factor of 3 to avoid flutter). The optimal ailerons deflection time history obtained is shown in Fig. 14, together with the actuation signal used as initial guess for the optimisation. As expected, in the first part of the manoeuvre ($t < 6$ s) the ailerons are fully deployed, so as to roll the wing as fast as possible and maximise the side force (Fig. 14b); in a second stage ($t > 6$ s), they deflect in the opposite direction, moving the system back to its initial configuration. Note, however, that this time the control can exploit the stabilising rolling to increase the rolling speed and, as a result, the time span during which the ailerons are at their maximum travel limit is reduced. As seen in the previous cases, even here the fast dynamics and the fact that an integral condition — second term in eq. (11) — was chosen to determine the final state of the system cause the ailerons to oscillate around zero for $t > T_s$; however, this has minimal impact in the resulting side force (Fig. 14b, $t > T_v$). During the

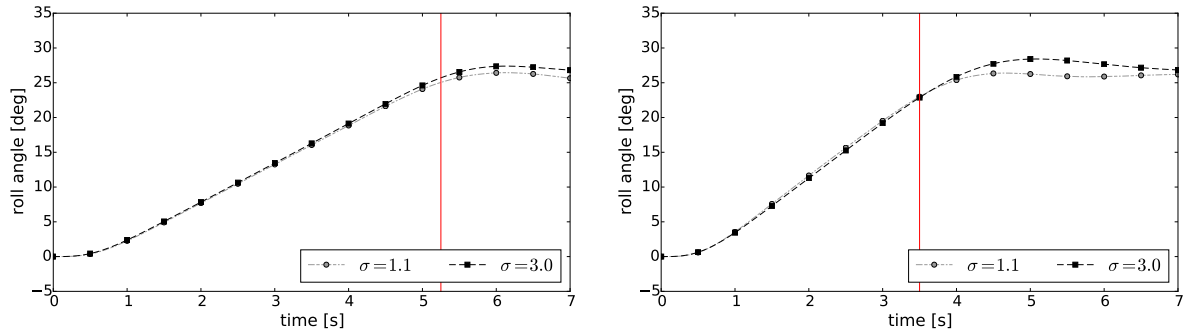

(a) $T_v = 75\%\ T$ (b) $T_v = 50\%\ T$

Figure 11: Roll attitude during the for optimal anti-symmetric actuation $\beta_L = -\beta_R$ obtained starting from a zero initial guess and using wings of different stiffness. The plots also show the time of average T_v.

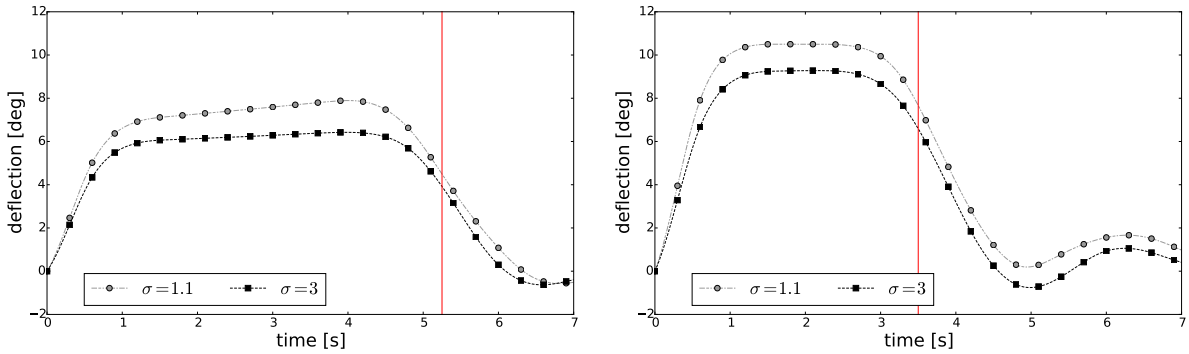

(a) $T_v = 75\%\ T$ (b) $T_v = 50\%\ T$

Figure 12: Optimal anti-symmetric actuation $\beta_L = -\beta_R$ for different levels of stiffness and zero initial guess.

manoeuvre, geometrical changes are large enough to impact the wing dynamical features (Sec. III.B). This is shown in Fig. 15a, where the tip vertical displacements magnitude reaches a maximum of 10 % of the half wing span.

IV. Conclusions

The single shooting method has been used to define the open-loop control laws of the control surfaces of very flexible hinged wings, with the objective of enhancing the system rolling performance. To account for large geometrical changes during the manoeuvre, the wing structure has been modelled via a GEBM and coupled with a UVLM aerodynamic model. The deflection time history of the control surfaces has been parametrised via a set of B-splines basis and the optimal actuation has been driven by a SLSQP algorithm.

In the first part of the work, key aspects of the rolling performance of flexible wings have been analysed. As the stiffness is reduced, it was shown that the fore-shortening effect connected to large bending deflection reduces the control surfaces authority. In comparison to rigid wings with no dihedral or sweep, however, flexible wings were found to be more stable. This was shown to be connected to a number of nonlinear features, such as changes in local angle of attack associated to bending and asymmetric deflections between starboard and port sides of the wing during rolling. The dihedral effect linked to bending was, instead, found to be particularly intense when the wing was allowed to move side-ways.

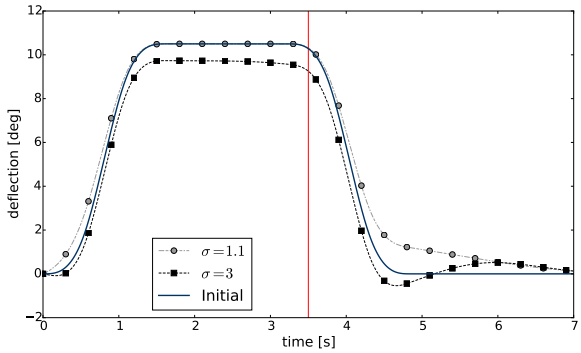

(a) $T_v = 75\%\ T$

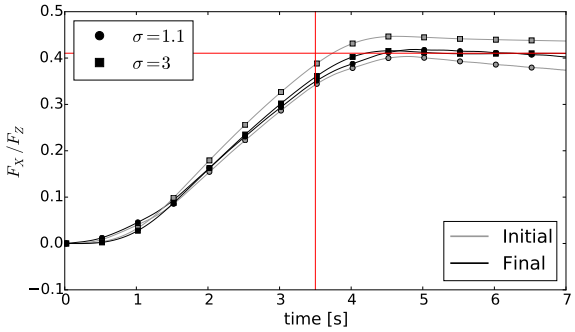

(b) $T_v = 50\%\ T$

Figure 13: Anti-symmetric ailerons deflection and aerodynamic side force obtained from a non zero initial guess and using wings of different stiffness. The plot also shows the target lateral force and the time of average T_v.

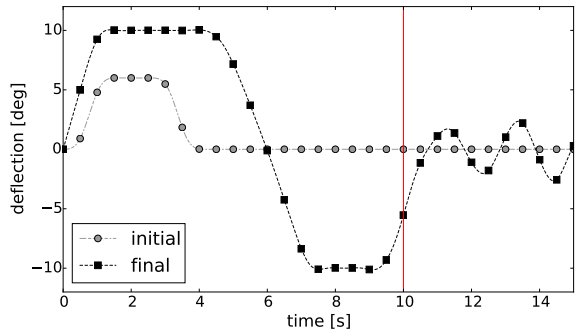

(a) Aileron deflection, $\beta_R = -\beta_L$

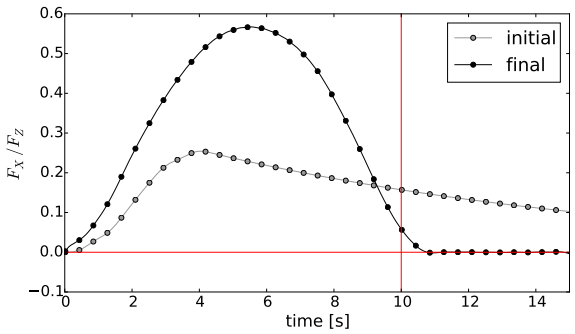

(b) Normalised side force

Figure 14: Optimal antisymmetric aileron deflection time history and side force obtained during the manoeuvre defined through the cost function in eq. (11).

Optimal actuation time histories for rolling have been finally designed starting from a zero initial guess. Regardless of the level of flexibility of the wing, the single shooting approach managed to capture the system features and lead to satisfactory results. Performance were, in particular, found to be comparable to those obtained using the optimisation for the refinement of an actuation law designed for rigid wings. While the robustness of the method when dealing with more complex dynamics still requires a further assessment, the approach, which can be easily extended to deal with the simultaneous wing/controller optimisation problem, has shown that optimal control provides a valuable tool to define actuation strategies in nonlinear aeroelastic wings.

Acknowledgements

The authors are grateful for the sponsorship of the UK Engineering and Physical Science Research Council (EPSRC).

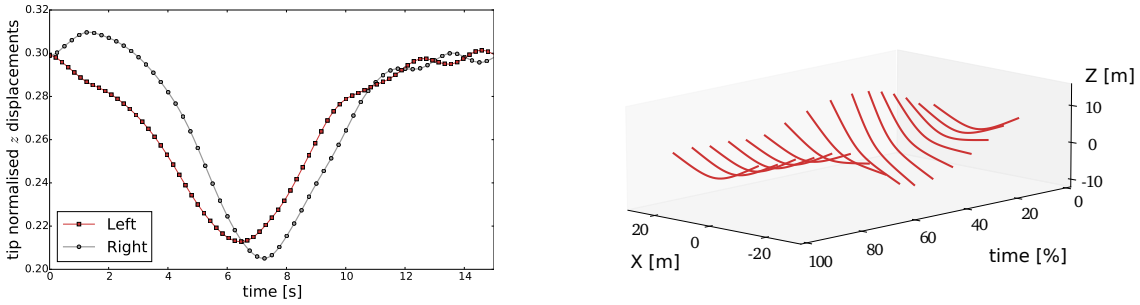

(a) Vertical tip displacements

(b) Snapshots

Figure 15: Vertical tip displacements (normalised with respect to the wing half span, L) and snapshots for the optimal manoeuvre defined through the cost function in eq. (11).

References

[1] Mukhopadhyay, V., "Historical Perspective on Analysis and Control of Aeroelastic Responses," *Journal of Guidance, Control, and Dynamics*, Vol. 26, No. 5, 2003, pp. 673–684.

[2] Cesnik, C. E., Palacios, R., and Reichenbach, E. Y., "Reexamined Structural Design Procedures for Very Flexible Aircraft," *Journal of Aircraft*, Vol. 51, No. 5, 2014, pp. 1580–1591.

[3] Patil, M. J. and Hodges, D. H., "Output Feedback Control of the Nonlinear Aeroelastic Response of a Slender Wing," *Journal of Guidance, Control, and Dynamics*, Vol. 25, No. 2, 2002, pp. 302–308.

[4] Tuzcu, I., Marzocca, P., Cestino, E., Romeo, G., and Frulla, G., "Stability and Control of a High-Altitude, Long-Endurance UAV," *Journal of Guidance, Control, and Dynamics*, Vol. 30, No. 3, 2007, pp. 713–721.

[5] Shearer, C. M. and S. Cesnik, C. E., "Trajectory Control for Very Flexible Aircraft," *Journal of Guidance, Control, and Dynamics*, Vol. 31, No. 2, 2008, pp. 340–357.

[6] Allison, J. T., Guo, T., and Han, Z., "Co-Design of an Active Suspension Using Simultaneous Dynamic Optimization," *Journal of Mechanical Design*, Vol. 136, No. 8, jun 2014, pp. 14.

[7] Lin, Q., Loxton, R., and Teo, K. L., "The Control Parameterization Method for Nonlinear Optimal Control: A Survey," *Journal of Industrial and Management Optimization*, Vol. 10, No. 1, 2013, pp. 275–309.

[8] Maraniello, S. and Palacios, R., "Co-Design of Very Flexible Actuated Structures," *International Forum on Aeroelasticity and Structural Dynamics*, Saint Petersburg, Russia, 2015, pp. 1–25.

[9] Murua, J., Palacios, R., and Graham, J. M. R., "Applications of the Unsteady Vortex-Lattice Method in Aircraft Aeroelasticity and Flight Dynamics," *Progress in Aerospace Sciences*, Vol. 55, 2012, pp. 46–72.

[10] Simpson, R. J. S., Palacios, R., and Murua, J., "Induced-Drag Calculations in the Unsteady Vortex Lattice Method," *AIAA Journal*, Vol. 51, No. 7, 2013, pp. 1775–1779.

[11] Hesse, H. and Palacios, R., "Reduced-Order Aeroelastic Models for Dynamics of Maneuvering Flexible Aircraft," *AIAA Journal*, Vol. 52, 2014, pp. 1–16.

[12] Patil, M. J. and Hodges, D. H., "On the Importance of Aerodynamic and Structural Geometrical Nonlinearities in Aeroelastic Behavior of High-Aspect-Ratio Wings," *Journal of Fluids and Structures*, Vol. 19, 2004, pp. 905–915.

[13] Patil, M. J., Hodges, D. H., and Cesnik, C. E. S., "Nonlinear Aeroelasticity and Flight Dynamics of High-Altitude Long-Endurance Aircraft," *Journal of Aircraft*, Vol. 38, No. 1, 2001, pp. 88–94.

[14] Murua, J., Hesse, H., Palacios, R., and Graham, J. M. R., "Stability and Open-Loop Dynamics of Very Flexible Aircraft Including Free-Wake Effects," *52nd AIAA Structures, Structural Dynamics, and Materials Conference*, Denver, Colorado, 2011.

[15] Hesse, H., Palacios, R., and Murua, J., "Consistent Structural Linearization in Flexible Aircraft Dynamics with Large Rigid-Body Motion," *AIAA Journal*, Vol. 52, No. 3, 2014, pp. 528–538.

[16] Hodges, D. H., "A Mixed Variational Formulation Based on Exact Intrinsic Equations for Dynamics of Moving Beams," *International Journal of Solids and Structures*, Vol. 26, No. 11, 1990, pp. 1253–1273.

[17] Geradin, M. and Cardona, A., *Flexible Multibody Dynamics: A Finite Element Approach*, John Wiley & Sons Ltd, Chichester, UK, 2001.

[18] Palacios, R., "Nonlinear Normal Modes in an Intrinsic Theory of Anisotropic Beams," *Journal of Sound and Vibration*, Vol. 330, No. 8, 2011, pp. 1772–1792.

[19] Martins, J. R. R. A. and Lambe, A. B., "Multidisciplinary Design Optimization: A Survey of Architectures," *AIAA Journal*, Vol. 51, No. 9, 2013, pp. 2049–2075.

[20] Schlegel, M., Stockmann, K., Binder, T., and Marquardt, W., "Dynamic Optimization Using Adaptive Control Vector Parameterization," *Computers & Chemical Engineering*, Vol. 29, No. 8, 2005, pp. 1731–1751.

[21] Fabien, B. C., "Piecewise Polynomial Control Parameterization in the Direct Solution of Optimal Control Problems," *Journal of Dynamic Systems, Measurement, and Control*, Vol. 135, No. 3, 2013.

[22] Kraft, D., "A Software Package for Sequential Quadratic Programming," Tech. rep., DLR German Aerospace Center Institute for Flight Mechanics, Köln, Germany, 1988.

[23] Smith, M. J., Patil, M. J., and Hodges, D. H., "CFD-Based Analysis of Nonlinear Aeroelastic Behaviour of High-Aspect Ratio Wings," *42nd AIAA/ASME/ASCE/AHS/ASC Structures, Structural Dynamics, and Material Conference and Exhibit*, AIAA 2001-1582, Seattle, WA, 2001, pp. 1–10.

[24] Peters, D. A. and Cao, W.-M., "Finite State Induced Flow Models Part I: Two-Dimensional Thin Airfoil," *Journal of Aircraft*, Vol. 32, No. 2, 1995, pp. 313–322.

[25] Tang, D. M. and Dowell, E. H., "Effects of Geometric Structural Nonlinearity on Flutter and Limit Cycle Oscillations of High-Aspect-Ratio Wings," *Journal of Fluids and Structures*, Vol. 19, 2004, pp. 291–306.